J Mol Model (2011) 17:1727–1734
DOI 10.1007/s00894-010-0881-7

ORIGINAL PAPER

Docking and molecular dynamics study on the inhibitory activity of *N, N*-disubstituted-trifluoro-3-amino-2-propanols-based inhibitors of cholesteryl ester transfer protein

Bo-Liang Dong · Qing-Hua Liao · Jing Wei

Received: 22 April 2010 / Accepted: 18 October 2010 / Published online: 6 November 2010

Abstract Extensive studies suggest direct links between cholesteryl ester transfer protein (CETP), high-density lipoproteins-cholesterol level and cardiovascular diseases. Many therapeutic approaches are aimed at the CETP. A series of *N, N*-disubstituted-trifluoro-3-amino-2-propanol analogues are among the most highly potent and selective inhibitors of CETP described to date. For in-depth investigation into the structural and chemical features responsible for exploring the binding pocket of these compounds, as well as for the binding recognition mechanism concerned, we performed a series of automated molecular docking operations. Moreover, the docking results were quite robust as further validated by molecular dynamics. The docking results reveal that the binding site mainly consists of two hydrophobic regions (P1 and P2 site) which are able to accommodate the lipophilic arms of the compounds investigated. Val421 in P1 site and Met194 in P2 site could be considered to be two important residues in forming the two hydrophobic regions. The presence of residues Phe197 and Phe463 in P2 site may be responsible for the binding recognition through π-π stacking interactions. The hydrophobic 3-phenoxy substituent may be important in creating the preferable inhibitive capability for increasing the binding potency. The hydrophobic character of the tetrafluoroethoxybenzyl group at position 3 displays better hydrophobicity than a shorter hydrophobic substituent. An interaction model of CETP-inhibitors is derived that can be successfully used to explain the different biologic activities of these inhibitors. It is anticipated that the findings reported here may provide very useful information or clues for designing effective drugs for the therapeutic treatment of CETP-related cardiovascular diseases.

Keywords Binding mechanism · CETP Inhibitors · Cholesteryl ester transfer protein · Molecular docking · Molecular dynamics

Abbreviations

CETP	Cholesteryl ester transfer protein
CE	Cholesteryl ester
HDL	High-density lipoproteins
LDL	Low-density lipoproteins
LDL-C	LDL-cholesterol
HDL-C	HDL-cholesterol
RMSD	Root-mean square deviation
MD	Molecular dynamics

Introduction

Cholesteryl ester transfer protein (CETP) is a hydrophobic glycoprotein [1] that is often bound to high-density lipoproteins (HDL) in circulation. CETP engages in the transfer of neutral lipids, including cholesteryl ester (CE) and triglyceride, among lipoprotein particles [2, 3]. The CETP-mediated transfer of CE from high-density lipoproteins to low-density lipoproteins (LDL) increases LDL-cholesterol (LDL-C) and lowers HDL-cholesterol (HDL-C).

Electronic supplementary material The online version of this article (doi:10.1007/s00894-010-0881-7) contains supplementary material, which is available to authorized users.

B.-L. Dong · Q.-H. Liao · J. Wei (✉)
Tianjin Key Laboratory for Modern Drug Delivery & High-Efficiency, School of Pharmaceutical Science and Technology, Tianjin University,
92 Weijin Road, Nankai District,
Tianjin 300072, People's Republic of China
e-mail: betty_wj@tju.edu.cn

Clinical trials indicate that low levels of HDL-C are an independent and important risk factor for cardiovascular diseases, the leading cause of death in many countries. CETP plays a potential antiatherogenic role in reverse cholesterol transport which helps remove CE from peripheral tissues to the liver [4–6].

In the past few years, multiple classes of synthetic inhibitors were identified to raise HDL-C levels, including tetrahydrochinolines [7], 2-arylbenzoxazoles [8, 9], dimethylpropanethioates [10], dibenzodioxocinones [11], tetrahydoquinoxalines [12], *N,N*-disubstituted trifluoro-3-amino-2-propanols [13, 14] derivatives. Most of the CETP inhibitors exhibit high IC_{50} values (exhibiting for inhibiting CETP-mediated transfer of ^{3}H-CE from HDL to LDL in human serum) with the micromolar range in human serum [15]. In all cases, further optimization of this activity could not be achieved, and analogues with millimicromole potency were proved to be elusive.

Understanding the interactions between inhibitors and their target receptor is an essential step in any pharmaceutical or chemical research program. Up to now, only the X-ray crystal structures of CETP and natural substrates have been reported [1]. The structure of CETP at 2.2-Å resolution reveals a 60-Å-long tunnel that traverses the core of the protein. The tunnel has two distinct openings: N-terminal and C-terminal domains. The two hydrophobic cholesteryl esters are buried in the middle of the continuous tunnel and an amphiphilic phosphatidylcholine plug is at each end. Figure 1 describes the structures of two hydrophobic cholesteryl esters with CETP.

However, the binding models of the inhibitors are still unknown. To solve this problem and provide new insights into the inhibitors-CETP interactions, a theoretical study employing the molecular docking and molecular dynamics approaches has been carried out. In our study, the inhibitors of *N, N*-disubstituted-trifluoro-3-amino-2-propanols were docked into the ligand binding pockets of CETP using the AutoDock program to explore the inhibitors-CETP interactions. The reliability of this CETP model was probed using molecular-dynamics simulations. Computer-aided simulation of protein-ligand interactions can often be of great help in guiding and interpreting experiments, and is helpful in providing atomic details that are inaccessible using other experimental techniques [16–19]. It is hoped that information from this study will provide further understanding of the interaction mechanism and enable the design of CETP inhibitors as cardiovascular drugs.

Materials and methods

The three-dimensional structure of CETP was retrieved from the Protein Data Bank as the docking receptor (http://www.rcsb.org/pdb; accession code 2OBD). Ten synthetic inhibitors of *N, N*-disubstituted-trifluoro-3-amino-2-propanols were chosen from published literature in this study [20]. Their structures and biologic activities (IC_{50} values) are shown in Table 1. All the CETP inhibitors were built using a 2D/3D editor-sketcher and were minimized to a local energy minimum using the CHARMm-like force field implemented within the Catalyst4.11 software [21].

AutoDock was recently reported to be the most popular docking program [22]. Its high accuracy and versatility have expanded its use [23, 24]. To explore the probable active sites of the CETP, flexible-ligand docking was initially performed using energetically optimized ligands at different potential binding sites of the whole protein (blind docking). The blind docking area was defined by the dimension of 126×126×126 points with grid spacing of 0.375 Å. The grid box was centered on the macromolecule and covered almost the whole tunnel of CETP. The docked results were ranked according to the binding free energy and were clustered on the basis of root-mean square deviation (RMSD). The conformations with the lowest docked energy was chosen from the most populated clusters and put through further analysis.

The further accurately docked analysis was carried out with the ligands in order to identify the structural basis for the specificity of the different ligands to inhibit HDL. The methods involved were similar to the blind docking, except that the grid box size was reduced to 60×60×60 points and centered on the ligand. The combination of docking modeling and experimental analysis can provide much detailed information speeding the docking process.

Both the CETP crystal structure and inhibitory ligands were prepared using AutoDock Tools v.1.5.2 software. All docking calculations were done with the AutoDock software package using the Lamarckian genetic algorithm (LGA). A population size of 300 and 25,000,000 energy evaluations were used for 200 and 50 search runs corresponding to the blind docking and accurate docking. The conformations from the docking experiments were analyzed using Chimera (a visualization system for exploratory research and analysis) [25], which also identifies the hydrophobic interactions between the receptor and the ligands.

Based on the docking results, molecular dynamics simulations for compound **1** were performed using the SANDER module, implemented in the Amber 10 package. The Amber parm99SB force field and the general AMBER force field (GAFF) [26] were respectively used for the protein and the ligands. All of the complexes were solvated using a shell of TIP3PBOX water model [27] with a closeness parameter of 10 Å away from the boundary of any protein and ligand atoms. All covalent bonds containing the hydrogen atoms were constrained using SHAKE

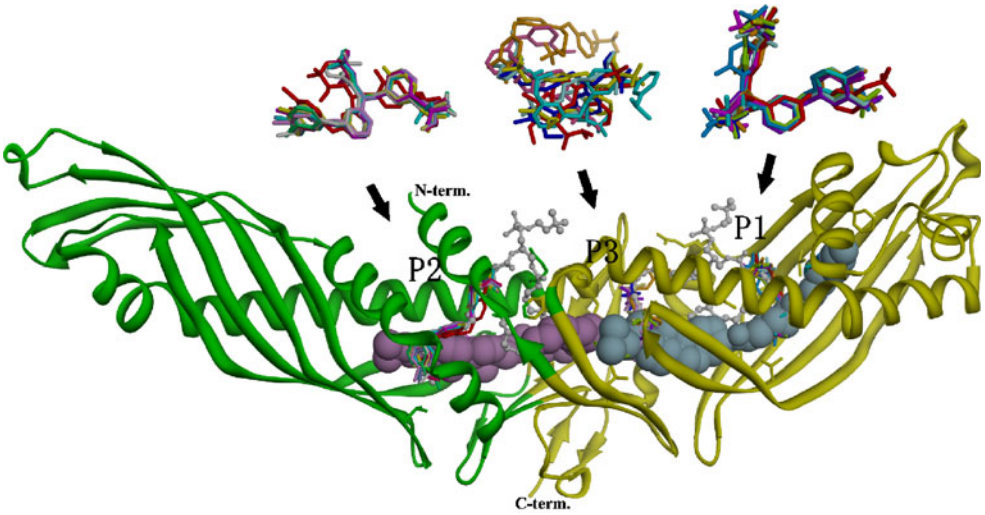

Fig. 1 Locations of the pockets calculated by docking approach. Ribbon diagram of the CETP is shown to emphasize the superimposition of the conformations of the ten inhibitors at the binding pocket P1, P2 and P3 sites; the overlapped ligands are clearly shown as sticks right above each pocket. It also shows the domains of N-terminal (green) and C-terminal (yellow)

algorithm [28]. The particle mesh Ewald method [29] was used to treat long-range electrostatic interactions. Energy minimization was used to release the bad contacts in the crystallographic structure, and the convergence criterion for the energy gradient was 0.0001 cal•mol^{-1}•Å^{-1}. Subsequently, the complexes of the minimized structures were subjected to 2600 ps molecular dynamics (MD) simulations at 300 K and 1 bar pressure with an integration step of 2 fs and NPT as an ensemble type. The interactions between the compound **1** and each residue in protein are analyzed using the MM-GBSA decomposition process applied in the MM-GBSA module in AMBER 10 package. The binding interaction of the inhibitor–residue pair includes three terms: van der Waals contribution (T_{vdw}), electrostatic

Table 1 In vitro inhibition of chiral R-enantiomers of phenoxy-substituted *N, N*-disubstituted-trifluoro-3-amino-2-propanols using recombinant human CETP in human seruma. Biologic activities and docking results of compounds **1**-**10** calculated with AutoDock 4.0. Structures of the ten CETP inhibitors also investigated in this study

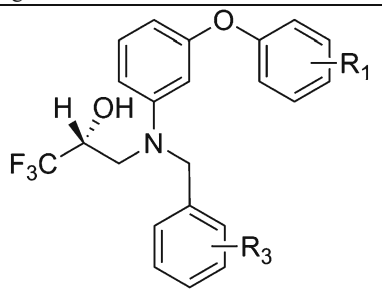

No.	R1	R2	IC_{50}[a]	$E_{binding}(E_{vdw-desol})$[b] (kcal/mol)		
				P1 site	P2 site	P3 site
1	4-chloro-3-ethyl	3-(1,1,2,2-tetrafluoroethoxy)	59	-12.01	-10.69	-9.35
2	H	3-(1,1,2,2-tetrafluoroethoxy)	640	-9.70	-9.12	-8.85
3	3-ethyl	3-(1,1,2,2-tetrafluoroethoxy)	72	-11.27	-10.59	-8.67
4	3-trifluoromethoxy	3-(1,1,2,2-tetrafluoroethoxy)	190	-10.85	-10.34	-8.66
5	4-methyl	3-(1,1,2,2-tetrafluoroethoxy)	620	-9.72	-9.25	-8.58
6	3-isopropyl	3-(1,1,2,2-tetrafluoroethoxy)	110	-11.25	-10.54	-9.33
7	4-chloro-3-ethyl	3-trifluoromethoxy	790	-9.57	-9.01	-8.79
8	4-chloro-3-ethyl	3-pentafluoroethyl	440	-10.05	-9.83	-9.24
9	4-chloro-3-ethyl	2-fluoro-5-trifluoromethyl	770	-9.60	-9.04	-9.19
10	4-chloro-3-ethyl	2-fluoro-4-trifluoromethyl	590	-9.91	-9.35	-9.20

[a] IC_{50} (nM) in human serum

[b] The consensus docking results are calculated in detail according to the protocol given in the supplementary information

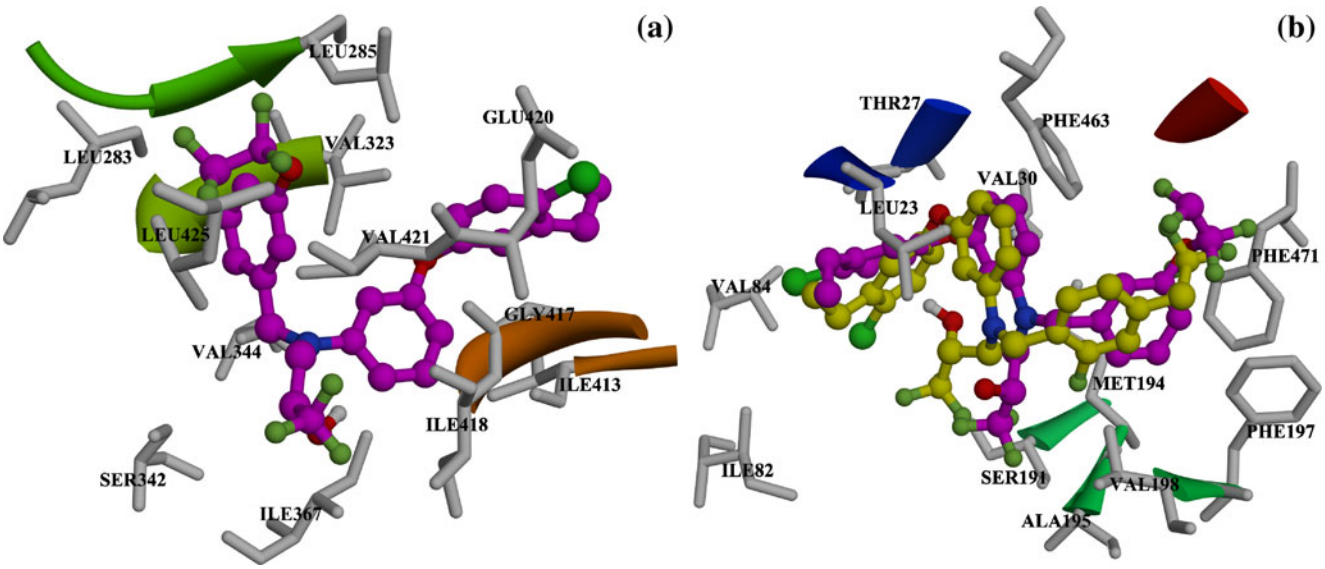

Fig. 2 A close view of the binding interaction of CETP with: (**a**) compound 1 (pink) in P1 site; (**b**) compound 1 (pink) and compound 10 (yellow) in P2 site

contribution (T_{ele}) and non-polar solvation contribution (T_{nonpol}). All energy components in Eq. (1) are calculated using the same snapshots as the free energy calculation.

$$\Delta G_{inhibitor-residue} = T_{vdw} + T_{ele} + T_{nonpol} \quad (1)$$

Results and discussion

Validation of AutoDock docking method

AutoDock was reported to be able to select the correct protein-ligand complexes, based on energy, without the prior knowledge of the binding site. A search for potential binding pockets [30] for compound **1** in the CETP was first carried out by 200 independent docking runs. The docking results reveal a set of different ligand conformations with the estimated binding free energy ranging from 10.14 kcal mol^{-1} to -5.31 kcal mol^{-1}.

We performed a clustering analysis to categorize the obtained ligand conformations into three clusters, except for six docking conformations outside the CETP protein. The most populated cluster (including 139 conformations) is positioned in a hydrophobic pocket close to N-terminal domain (called as P1 site), Fig. 1. P1 site is mainly formed by the side chains of Leu283, Leu285, Val323, Ser342, Val344, Ile367, Ile413, Gly417, Ile418, Glu420, Val421 and Leu425 (as shown in Fig. 2a). The second populated cluster is located near the C-terminal domain that is referred to as P2 site. The surrounding residues of P2 site are Leu23, Thr27, Val30, Ile82, Val84, Ser191, Met194, Ala195, Phe197, Val198, Phe463 and Phe471 (as shown in Fig. 2b). The third cluster is located on a scattering region between P1 and P2. This region is named P3 site. All docking conformations are distributed in the P1~P3 sites with the frequencies of occurrence of 43%, 41% and 13%, respectively. The relative estimated binding free energy of the most favorable conformation in each cluster is -10.14, -9.60 and -8.57 kcal mol^{-1}, respectively.

Ten *N, N*-disubstituted trifluoro-3-amino-2-propanols analogues were accurately docked within the P1~P3 sites of CETP. The conformations with the most favorable free binding energy in the P1~P3 sites were respectively selected from accurate docking analogues as the optimal docked conformations. Figure 1 shows the superimposition of their conformations at the three binding pockets. Table 1 shows their (for the conformations) IC_{50} values, related to their experimental biologic activities, and the results obtained by the molecular docking operation. Moreover, the linear regression was performed between the calculated binding free energies and experimental biologic activities. Both results in P1 and P2 sites indicate an excellent correlation (R^2=0.970 and R^2=0.931) between the properties cited above. Figure 3 shows this relationship in P1 site and P2 site. However, a poor correlation (R^2=0.090) was obtained concerning the cited properties for the compounds in P3 site. In addition, docking of the ligands into the P3 binding pocket did not converge toward a single binding position. Based on the reasons mentioned above, it is considered that the P3 site does not necessarily represent the binding mode with respect to the P1 and P2 sites generated by docking software. So we described the binding modes in the P1 and P2 sites as follows.

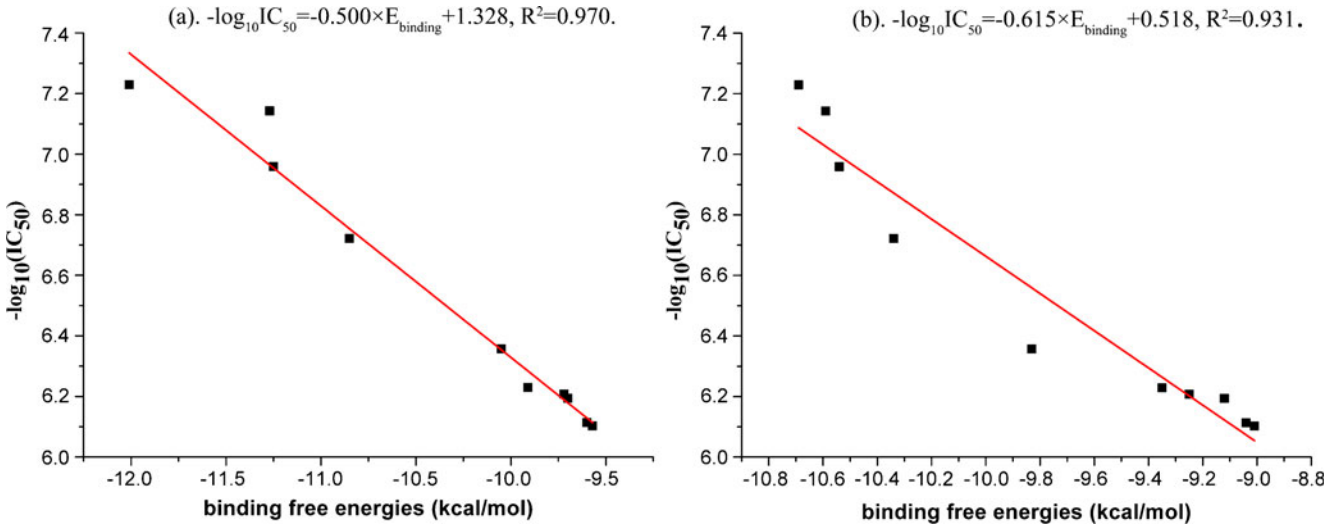

Fig. 3 Relationship obtained by performing the linear regression between the binding free energy and the biological activity ($-\log_{10}IC_{50}$) for the inhibitors 1-10, in P1 site (**a**), and in P2 site (**b**)

Binding model

The ten compounds have quite similar structures and are generally positioned in the P1 or P2 binding pocket with essentially the same mode. As shown in the Electronic supplementary material (ESM), the presence of hydrophobic energy (non-polar energy) in all the ligands is not of little importance but essential to the binding energy of the ligands. To illustrate the binding modes, the compound **1** is used as a paradigm to probe the hydrophobic interactions between inhibitors and CETP. This compound is chosen owing to the highest binding energy, (Table 1). The amino acids within 5 Å (in both P1 and P2 sites) of the docked ligand **1** are shown in Fig. 2.

In the P1 site, the shape of the binding pocket is observed to complement the pose of the ligand (shown in Fig. 2a). The tetrafluoroethoxy is protruded out toward the surface of the protein, while the rest of the molecule is embedded into the inner part of the protein. The tetrafluoro-substituted phenyl ring of the ligand faces toward the tunnel openings in C-terminal and is stabilized with a strong hydrophobic interaction to the main residues Leu283, Leu285, Val344 and Leu425. The binding mode reveals that the trifluoro-3-amino-2-propanols have the hydrophobic interactions with the surrounding amino acid residues of the C-terminal region, such as residues Ser342, Ile367, Ile418 and Val421. The 4-chloro-3-ethylphenoxy substituent fits in a hydrophobic glove formed by the Val323, Ile413, Gly417 and Glu420. This binding mode may have critical structural effect on the hydrophobic region in promoting the inhibitory processing.

In the P2 site, the 4-chloro-3-ethylphenoxy group is inserted deeply in the tunnel, forming a hydrophobic contact with the residues Leu23, Thr27, Val30, Ile82 and Val84. Also the benzene ring of aniline produces a T-shape π-π stacking interaction with the benzene ring on Phe463. The extra π-π stacking interaction results in the satisfactory binding affinity. The docking study proves that the trifluoro-3-amino-2-propanol is buried in a hydrophobic cavity constituted of residues Ser191, Met194 and Met195. The tetrafluoroethoxybenzyl group of the ligand faces toward the tunnel openings in N-terminal. The tetrafluoro-group is located in the hydrophobic pocket formed by Phe197, Val198, Phe463 and Leu471. The benzene ring of tetrafluoroethoxybenzyl group produces the extra π-π stacking interaction with residues Phe197. Presumably, π-π stabilizing interactions between the benzene ring and its surrounding residues Phe197 are confined to a region which may impose significant conformational change to the ligands.

Structure-activity relationship

Note that, the docking scores are very sensitive and the slight positional difference is detectable in the scores. The docking studies performed gave better structural insights and understanding on how the various ligands interacted with the CETP protein in acting as competitive inhibitors. Analysis of the structure-activity relationships of the ligands may shed light on the important structure and conformation which could be applied in the design of new compounds.

A 4-methyl group or 4-hydrogen atom of the phenoxy substituent to yield compound **2** and compound **5** results in a great loss of the binding energy obtained from the Autodock scoring function. The observations are in agreement with the experimental results. This result suggests that the hydrophobic substituent at 3-phenoxy

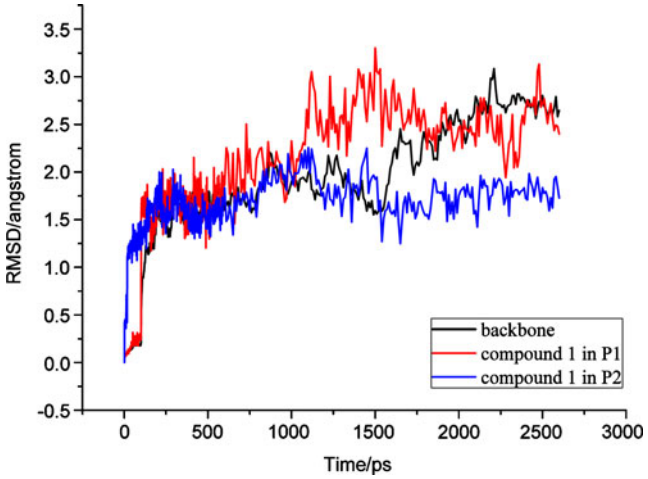

Fig. 4 Root mean square deviation (RMSD) obtained during the 2600 ps MD simulation for the backbone of CETP and compound 1 in both P1 and P2 sites. The deviation is with respect to the corresponding starting structure as a function of time

group plays an important role in the binding activity of the ligands. The binding energies of compound **7** and **8** drop to -9.57/-10.05 kcal mol^{-1} in P1 and -9.01/-9.83 kcal mol^{-1} in P2 corresponding to -12.01 and -10.69 kcal mol^{-1} in compound **1**, (Table 1). The reductive energies are predominantly due to the decrease of hydrophobic interactions with Leu283 in P1, Leu425 in P1 and Phe463 in P2. Investigation into structure-activity relationship suggests that the shorter substituent at 3-phenoxy group in inhibitors **7** and **8** will weaken hydrophobic capability. In compound **9** and **10**, the introduction of *o*-fluorine substituent at benzyl group results in the steric hindrance with residue Phe471. Obviously, the unfavorable hindrance changes the spatial conformation and the binding site direction of the 4-trifluoromethylbenzyl chain, as shown in Fig. 2b. The effects of ligand binding vary with the degree of hydrophobic interactions in the system, contributing to the determination of the docking energies.

In this sense, the larger volume of the sulfur atom compared to the oxygen is in a region of the receptor that is free in active compounds, being about 2.5 Å from residues Met121 and Val125, yielding to steric hindrance and close contacts.

Molecular dynamics

In order to verify whether the results obtained here by docking are a robust or a fortuitous results, we carried out a 2.6 ns molecular dynamics simulation with the highly active compound **1** that presented the different binding modes with CETP according to AutoDock. The main purpose is to investigate the positional and conformational changes of inhibitors relative to the active pocket and the specialty pocket residues and further reveals the binding stability.

According to the 2.6 ns MD simulation for the structures of two CETP inhibitors, the system became equilibrated

Table 2 Decomposition of $\Delta G_{inhibitor-residue}$ on a per-residue basis[a]

Residues	T_{vdw} (kcal/mol)	T_{ele} (kcal/mol)	T_{nonpol} (kcal/mol)	$\Delta G_{inhibitor\text{-}residue}$[b] (kcal/mol)
in P1 site				
Leu283	-1.69	-0.28	0.54	-1.43 (0.00)
Leu285	-1.34	-0.17	0.26	-1.24 (0.01)
Val323	-1.74	-0.03	-0.2	-1.96 (0.01)
Ser342	-0.62	-2.08	1.38	-1.32 (0.00)
Val344	-1.48	-0.02	-0.24	-1.75 (-0.01)
Ile367	-1.46	-0.28	0.2	-1.53 (0.01)
Ile413	-1.46	-0.02	0.2	-1.29 (-0.01)
Gly417	-1.8	0.32	0.32	-1.16 (0.00)
Ile418	-1.23	0.23	-0.1	-1.11 (-0.01)
Glu420	-0.82	1.04	-1.24	-1.02 (0.00)
Val421	-2.91	-0.23	-0.17	-3.31 (0.00)
Leu425	-1.04	-0.1	0.13	-1.01 (0.00)
in P2 site				
Leu23	-1.83	-0.16	0.39	-1.60 (0.00)
Thr27	-1.52	-0.37	0.24	-1.65 (0.00)
Val30	-1.09	0.03	-0.1	-1.16 (0.00)
Met194	-2.43	-1.2	1.57	-2.06 (0.00)
Phe197	-1.39	0.24	0.1	-1.05 (0.00)
Val198	-1.82	0.21	-0.06	-1.67 (0.00)
Phe463	-1.33	-0.3	0.59	-1.04 (0.00)

[a] Energies shown as contributions from van der Waals energy (T_{vdW}), the non-polar solvation energy (T_{nonpol}), the sum of the electrostatic energy (T_{ele}) and the sum of them ($\Delta G_{inhibitor—residue}$) of protein–inhibitor complex. All values are given in kcal mol^{-1}

[b] $\Delta G_{inhibitor—residue} = T_{vdw} + T_{ele} + T_{nonpol}$, the values in parentheses represent the standard errors which are a very small number and can be omitted in most cases

judged by RMSDs. The RMSDs of inhibitor relative to CETP and backbone of the receptor to its original conformation were calculated and outlined in Fig. 4. It can be seen that the receptor and compound **1** in the two pockets become stable after 1.6 ns in system with a mean RMSD value of 2.54 Å for the backbone, 2.51 Å for compound **1** in P1 and 1.73 Å for compound **1** in P2. So the three trajectories exhibit low backbone RMSD values (about 2.54 Å), which is indicative of stability. In addition, the stability of the system also proved the credibility of the docking results.

To assess the quality of our MD simulations, energetic and structural properties are monitored during the entire MD simulation of each complex. In the protein–inhibitor complexes, the electrostatic energies, non-polar solvation energies and van der Waals interactions are the basis for favorable binding free energies. Table 2 further illustrates the contributions of per residue (inhibitor–residue interaction larger than about 1 kcal mol^{-1}) in the binding site. The major binding attractions come from about 12 residues in P1 and seven residues in P2.

As shown in Table 2, the main forces which drive the binding of compound **1** to CETP channel are the van der Waals interactions. For Val421 and Met194 residues, the inhibitor–residue energies are more favorable than other residues for the binding, corresponding to -3.31 and -2.06 kcal mol^{-1}. As mentioned in the binding model section, Val421 and Met194 have hydrophobic interactions with the trifluoro-3-amino-2-propanol substituent, respectively. This phenomenon suggests the trifluoro-3-amino-2-propanol substituent plays an important role in the binding activity.

Conclusions

In this study, we used automated molecular docking to study the binding mechanisms for a series of *N,N*-disubstituted trifluoro-3-amino-2-propanol inhibitors. The predicted binding affinities are well correlated with the activities of these inhibitors. The docking results have been further validated as robust by the molecular dynamics simulation.

All these inhibitors mainly occupy the binding pockets of CETP with two different binding orientations (corresponding to P1 and P2 sites). Two binding sites composed mostly of hydrophobic amino acids are able to accommodate the lipophilic arms of the compounds concerned. The P1 pocket comprises mainly residues Leu283, Leu285, Val323, Ser342, Val344, Ile367, Ile413, Gly417, Ile418, Glu420, Val421 and Leu425. The P2 pocket includes mainly residues Leu23, Thr27, Val30, Ile82, Val84, Ser191, Met194, Ala195, Phe197, Val198, Phe463 and Phe471. The Phe463 forms a T-shape π-π stabilizing interaction with the ligands in P2. The benzene ring of tetrafluoroethoxybenzyl group is buried in the hydrophobic pocket containing Phe197, also leading to π-π stabilizing interactions. We also speculate that Met194 and Val421 establish favorable hydrophobic contacts with trifluoro-3-amino-2-propanol in both pockets. The presence of the trifluoro-3-amino-2-propanol in all the ligands is essential to the binding activity.

In these two sites, the more hydrophobic 3-phenoxy substituent may be preferable to the more inhibitive capability. Visualization of the selected 3-tetrafluoroethoxybenzyl group shows that, replacing this substituent with a shortened one, functionality reduced the hydrophobic interactions in both pockets. The benzylic *m*-substituent without an *o*-fluorine is characterized by lower steric hindrance than when it is in the *p*-position with an *o*-fluorine.

The findings may provide useful clues or stimulate new strategies for designing more effective drugs to inhibit CETP-related cardiovascular diseases. Accordingly, the docking results can not only predict the relative binding affinity of the CETP inhibitors but also address the binding affinity differences in terms of interaction distributions.

References

1. Qiu X, Mistry A, Ammirati MJ, Chrunyk BA et al (2007) Crystal structure of cholesteryl ester transfer protein reveals a long tunnel and four bound lipid molecules. Nat Struct Mol Biol 14:106–113
2. Okamoto H, Miyai A, Sasase T, Furukawa N, Matsushita M, Nakano T, Nakajima K (2007) Cholesteryl ester transfer protein promotes the formation of cholesterol-rich remnant like lipoprotein particles in human plasma. Clin Chim Acta 375:92–98
3. Zhou H, Li Z, Silver DL, Jiang XC (2006) Cholesteryl ester transfer protein (CETP) expression enhances HDL cholesteryl ester liver delivery, which is independent of scavenger receptor BI, LDL receptor related protein and possibly LDL receptor. Biochim Biophys Acta, Mol Cell Biol Lipids 1761:1482–1488
4. Polk D, Shah PK (2007) Cholesterol ester transfer protein (CETP) and atherosclerosis. Drug Discov Today: Ther Strateg 4:137–145
5. Schaefer EJ, Asztalos BF (2007) Increasing high-density lipoprotein cholesterol, inhibition of cholesteryl ester transfer protein, and heart disease risk reduction. Am J Cardiol 100:25–31
6. Quintão ECR, Cazita PM (2009) Lipid transfer proteins: past, present and perspectives. Atherosclerosis 209:1–9
7. Schmeck C, Gielen-Haertwig H, Vakalopoulos A, Bischoff H, Li V, Wirtz G, Weber O (2010) Novel tetrahydrochinoline derived CETP inhibitors. Bioorg Med Chem Lett 20:1740–1743
8. Hunt JA, Gonzalez S, Kallashi F, Milton L et al (2010) 2-Arylbenzoxazoles as CETP inhibitors: Substitution and modification of the a-alkoxyamide moiety. Bioorg Med Chem Lett 20:1019–1022
9. Smith CJ, Ali A, Chen L, Milton L et al (2010) 2-Arylbenzoxazoles as CETP inhibitors: substitution of the benzoxazole moiety. Bioorg Med Chem Lett 20:346–349
10. Maeda K, Okamoto H, Shinkai H (2004) S-(2-(Acylamino) phenyl) 2, 2-dimethylpropanethioates as CETP inhibitors. Bioorg Med Chem Lett 14:2589–2591

11. Bruckner D, Hafner FT, Li V et al (2005) Dibenzodioxocinones - a new class of CETP inhibitors. Bioorg Med Chem Lett 15:3611–3614
12. Eary CT, Jones ZS, Groneberg RD, Burgess LE et al (2007) Tetrazole and ester substituted tetrahydoquinoxalines as potent cholesteryl ester transfer protein inhibitors. Bioorg Med Chem Lett 17:2608–2613
13. Durley RC, Grapperhaus ML, Hickory BS et al (2002) Chiral N, N-disubstituted trifluoro-3-amino-2-propanols are potent inhibitors of cholesteryl ester transfer protein. J Med Chem 45:3891–3904
14. Connolly DT, Witherbee BJ, Melton MA, Durley RC et al (2000) Stereospecific inhibition of CETP by chiral N, N-disubstituted trifluoro-3-amino-2-propanols. Biochemistry 39:13870–13879
15. Sikorski JA (2006) Oral Cholesteryl Ester Transfer Protein (CETP) inhibitors: a potential new approach for treating coronary artery disease. J Med Chem 49:1–22
16. Wang SQ, Du QS, Huang RB, Zhang DW, Chou KC (2009) Insights from investigating the interaction of oseltamivir (Tamiflu) with neuraminidase of the 2009 H1N1 swine flu virus. Biochem Biophys Res Commun 386:432–436
17. Chou KC, Wei DQ, Zhong WZ (2003) Binding mechanism of coronavirus main proteinase with ligands and its implication to drug design against SARS. (Erratum: ibid., 2003, Vol. 310, 675). Biochem Biophys Res Commun 308:148–151
18. Wang SQ, Du QS, Chou KC (2007) Study of drug resistance of chicken influenza A virus (H5N1) from homology-modeled 3D structures of neuraminidases. Biochem Biophys Res Commun 354:634–640
19. Chou KC (2004) Insights from modelling the 3D structure of the extracellular domain of alpha7 nicotinic acetylcholine receptor. Biochem Biophys Res Commun 319:433–438
20. Reinhard EJ, Wang JL, Durley RC, Fobian YM, Margaret L et al (2003) Discovery of a simple picomolar inhibitor of cholesteryl ester transfer protein. J Med Chem 46:2152–2168
21. Catalyst version 4.10 (software package) (2005) Accelrys Inc, San Diego, USA
22. Sousa SF, Fernandes PA, Ramos MJ (2006) Protein-ligand docking: current status and future challenges. Proteins 65:15–26
23. Huang RB, Du QS, Wang CH, Chou KC (2008) An in-depth analysis of the biological functional studies based on the NMR M2 channel structure of influenza A virus. Biochem Biophys Res Commun 377:1243–1247
24. Du QS, Huang RB, Wang CH, Li XM, Chou KC (2009) Energetic analysis of the two controversial drug binding sites of the M2 proton channel in influenza A virus. J Theor Biol 259:159–164
25. Pettersen EF, Goddard TD, Huang CC, Couch GS, Greenblatt DM, Meng EC, Ferrin TE (2004) UCSF Chimera–a visualization system for exploratory research and analysis. J Comput Chem 25:1605–1612
26. Cornell WD, Cieplak P, Bayly CI, Gould IR, Kollman PA et al (1995) A second generation force field for the simulation of proteins, nucleic acids, and organic molecules. J Am Chem Soc 117:5179–5197
27. Jorgensen WL, Chandrasekhar J, Madura JD, Impey RW, Klein ML (1983) Comparison of simple potential functions for simulating liquid water. J Chem Phys 79:926–935
28. Ryckaert JP, Ciccotti G, Berendsen HJC (1977) Numerical integration of the Cartesian equations of motion of a system with constraints: molecular dynamics of n-alkanes. J Comput Phys 23:327–341
29. Darden T, York D, Pedersen L (1993) Particle mesh Ewald: An N. log(N) method for Ewald sums in large systems. J Chem Phys 98:10089–10092
30. Chou KC, Watenpaugh KD, Heinrikson RL (1999) A Model of the complex between cyclin-dependent kinase 5 (Cdk5) and the activation domain of neuronal Cdk5 activator. Biochem Biophys Res Commun 259:420–428